

The Role of Convection in Determining the Ejection Efficiency of Common Envelope Interactions

E. C. Wilson^{1*} and J. Nordhaus^{1,2,†}

¹Center for Computational Relativity and Gravitation, Rochester Institute of Technology, NY 14623, USA

²National Technical Institute for the Deaf, Rochester Institute of Technology, NY 14623, USA

Accepted XXX. Received YYY; in original form ZZZ

ABSTRACT

A widely used method for parameterizing the outcomes of common envelopes (CEs) involves defining an ejection efficiency, $\bar{\alpha}_{\text{eff}}$, that represents the fraction of orbital energy used to unbind the envelope as the orbit decays. Given $\bar{\alpha}_{\text{eff}}$, a prediction for the post-CE orbital separation is then possible with knowledge of the energy required to unbind the primary’s envelope from its core. Unfortunately, placing observational constraints on $\bar{\alpha}_{\text{eff}}$ is challenging as it requires knowledge of the primary’s structure at the onset of the common envelope phase. Numerical simulations have also had difficulties reproducing post-CE orbital configurations as they leave extended, but still bound, envelopes. Using detailed stellar interior profiles, we calculate $\bar{\alpha}_{\text{eff}}$ values for a matrix of primary-companion mass pairs when the primary is likely to incur a CE, i.e. at maximal extent in its evolution. We find that the ejection efficiency is most sensitive to the properties of the surface-contact convective region (SCCR). In this region, the convective turnover times are short compared to orbital decay timescales, thereby allowing the star to effectively radiate orbital energy and thus lower $\bar{\alpha}_{\text{eff}}$. The inclusion of convection in numerical simulations of CEs may resolve the ejection problem without the need for additional energy sources as the orbit must shrink substantially further before the requisite energy can be tapped to drive ejection. Additionally, convection leads to predicted post-CE orbital periods of less than a day, an observational result that has been difficult to reproduce in population studies where $\bar{\alpha}_{\text{eff}}$ is taken to be constant. Finally, we provide a simple method to calculate $\bar{\alpha}_{\text{eff}}$ if the properties of the SCCR are known.

Key words: binaries: general – stars: AGB and post-AGB – planet-star interactions – convection

1 INTRODUCTION

Common envelopes (CEs) are events that often occur in binary systems when one component, the primary, evolves off the main-sequence (Paczynski 1976; Ivanova et al. 2013; Kochanek et al. 2014). Significant radial expansion of the primary during post-main-sequence evolution can lead to direct engulfment of the companion, Roche Lobe overflow, and/or orbital decay via tidal dissipation (Nordhaus and Blackman 2006; Nordhaus et al. 2010; Chen et al. 2017). The result is a binary system consisting of the primary’s core and the companion embedded in a CE formed from the primary’s envelope.

Once immersed inside a CE, the orbit of the system decays rapidly ($\lesssim 1-1000$ years) making direct detection difficult (Ivanova et al. 2013) and precursor emission signatures a promising means of identification (MacLeod et al. 2018). Common envelope phases are

thought to be the primary mechanism for producing short-period binaries in the universe (Toonen and Nelemans 2013; Kruckow et al. 2018; Canals et al. 2018), though not the only method (Fabrycky and Tremaine 2007; Thompson 2011; Shappee and Thompson 2013).

During inspiral, energy and angular momentum are transferred from the orbit to the envelope (Iben and Livio 1993). If sufficient to eject the CE, a tight binary emerges that contains at least one compact object. If the envelope cannot be ejected, the companion is destroyed leaving a “single” star that nevertheless underwent a binary interaction such that its evolution may be modified (Nordhaus et al. 2011).

A method for parameterizing the outcomes of common envelopes, and hence predictions for their progeny populations, involves defining an ejection efficiency, $\bar{\alpha}_{\text{eff}}$, based on energetic arguments. This “ α -formalism” is broadly used in population synthesis studies and often defined in the following way:

$$\bar{\alpha}_{\text{eff}} = E_{\text{bind}}/\Delta E_{\text{orb}}, \quad (1)$$

* E-mail: ecw7497@rit.edu

† E-mail: nordhaus@astro.rit.edu

where E_{bind} is the energy required to unbind the primary’s envelope from its core and ΔE_{orb} is the orbital energy released during inspiral (for a detailed discussion see Sec 2.2; Tutukov and Yungelson 1979; Iben, I. and Tutukov 1984; Webbink 1984; Livio and Soker 1988; De Marco et al. 2011). Given $\bar{\alpha}_{\text{eff}}$, and knowledge of the primary’s binding energy, the post-CE orbital separations can then be determined. Because the transfer of energy to the envelope is not perfectly efficient, and because predictions for the progeny populations are highly sensitive to adopted values (Claeys et al. 2014), better constraints on $\bar{\alpha}_{\text{eff}}$, from either observations or theory, are topics of active research. In particular, an improved understanding of the ejection efficiency as a function of binary parameters or internal CE structure is needed as $\bar{\alpha}_{\text{eff}}$ is often taken to be constant.

Observations of CE progenitors have allowed some estimates of $\bar{\alpha}_{\text{eff}}$, albeit with significant uncertainties. Zorotovic et al. (2010) identified over 50 systems that are likely progeny of CE evolution, and determined that most are consistent with $\bar{\alpha}_{\text{eff}} \sim 0.2 - 0.3$. This is in general agreement with Cojocaru et al. (2017), who performed population synthesis studies of Galactic white dwarf main-sequence binaries using data from the Sloan Digital Sky Survey (SDSS) Data Release 12. Also utilizing population synthesis techniques, Davis et al. (2010) determined that $\bar{\alpha}_{\text{eff}} > 0.1$ reasonably describes all systems with late-type secondaries, but produced an overabundance of post-CE systems with orbital periods greater than a day. In a similar manner, Toonen and Nelemans (2013) argue that the ejection efficiency must be low to explain the observed post-CE orbital period distribution present in the SDSS sample.

Additional studies that have tested the dependence of the ejection efficiencies on the mass ratio of the binary, $q = m_2/M_1$, have produced conflicting results. De Marco et al. (2011) find that the mass ratio is in anti-correlation with $\bar{\alpha}_{\text{eff}}$; an increased companion mass results in a decreased $\bar{\alpha}_{\text{eff}}$. Zorotovic et al. (2011), by way of orbital separation, find that the mass ratio is in fact in correlation with $\bar{\alpha}_{\text{eff}}$, attributing the increased ejection efficiency to the increased initial orbital energy of the more massive companion. We discuss these contradictory findings in relation to our results in Section 4.

Three-dimensional hydrodynamic simulations of common envelopes have been carried out in recent years by multiple groups using diverse codes and numerical techniques (Ricker and Taam 2012; Passy et al. 2012; Ohlmann et al. 2016; Chamandy et al. 2018a). While inspiral occurs rapidly, the envelope is pushed outward yet remains bound. This failure to eject the CE has resulted in proposed solutions that include additional energy sources (recombination/accretion/jets), processes that operate on longer-timescales, or ejection through dust-driven winds (Soker 2015; Ivanova et al. 2015; Kuruwita et al. 2016; Glanz and Perets 2018; Sabach et al. 2017; Grichener et al. 2018; Kashi and Soker 2018; Ivanova 2018; Soker et al. 2018). While such effects may in fact prove necessary, it is first useful to consider the physical effects incorporated in simulations. The energy budget of the CE interaction is set by the initial orbital energy. As inspiral occurs, liberated orbital energy will be transferred to the CE unless it is lost via radiation. In this context, it is interesting to note that hydrodynamic simulations do not include radiation, and therefore should transfer 100% of the orbital energy to the gas in some form if energy is conserved, and thus cannot determine the efficiency. A full analysis of the energy components in CE simulations and a robust discussion of why the envelope remains bound at large distances is needed, i.e. Chamandy et al. (2018b).

There have been several previous studies that investigate the effects of convection in conjunction with recombination energy.

Grichener et al. (2018) in particular consider a common envelope in which the inspiraling companion deposits energy and the envelope expands. The authors find that convection efficiently transports recombination energy to surface radiative regions where it is lost. The energy transport time is on the order of months and shorter than dynamical timescales. This is consistent with the results we present in this work. In an earlier study, Sabach et al. (2017) argue that when helium recombines, energy transport by convection cannot be neglected. While it may increase the luminosity of the event, it cannot be used to unbind the envelope. Whether recombination energy can be tapped to drive ejection remains a subject of vigorous debate (Soker et al. 2018; Ivanova 2018).

In this paper, we focus on the general effects of convection, internal structure, and mass ratio on ejection efficiencies. Post-main sequence giants possess deep and vigorous convective envelopes which can carry energy to the surface where it can be lost via radiation, effectively lowering the ejection efficiency. In regions where radiative losses do not occur, convection can redistribute energy, carrying it to parcels of gas that are not in the direct vicinity of the binary, thus aiding ejection.

In Section 2, we describe our methodology, stellar models and the physics in which we ground our analysis. Our data are presented in Section 3. In Section 4 we discuss our results in the context of observational and theoretical work, and present our conclusions in Section 5.

2 METHODOLOGY

Our stellar models were computed using MESA (release 10108), an open-source stellar evolution code that allows users to produce spherically symmetric models of stellar interiors during all phases of a star’s evolution (Paxton et al. 2011, 2018)¹. Each star was evolved from the pre-main sequence to the white dwarf phase for zero-age-main-sequence (ZAMS) masses in the range of $0.8M_{\odot} - 6.0M_{\odot}$ in increments of $0.2M_{\odot}$ with finely-meshed time-stepping. Stars with initial masses below $0.8M_{\odot}$ were not included as they have not evolved off the main sequence during the lifetime of the universe. Mass loss on the Red Giant Branch (RGB) followed a Reimer’s prescription with $\eta_{\text{R}} = 0.7$ while mass loss on the Asymptotic Giant Branch (AGB) followed a Blocker prescription with $\eta_{\text{B}} = 0.7$ (Reimers 1975; Bloeker 1995). All models were assumed to have solar metallicity.

For each evolutionary model, the interior profile at maximum extent was chosen as this is the most likely time for a companion to be engulfed. When the star is fully extended, it occupies its maximum spatial volume. This allows for strong tidal torques which shrink the companion’s orbit. (Villaver and Livio 2009; Nordhaus et al. 2010; Nordhaus and Spiegel 2013). Each interior profile contains radial information about the mass, density, convective properties, and core and envelope boundaries. From these, we calculate the primary’s binding energy, location of the convective zones, inspiral timescales, tidal disruption radii, and the energy released during orbital decay. These quantities are used to determine $\bar{\alpha}_{\text{eff}}$ and the post-CE orbital separations for the companions that survive the CE interaction.

¹ MESA is available at <http://mesa.sourceforge.net>

2.1 Convective Regions

Post-main sequence stars host deep convective envelopes that can transport energy to optically thin surfaces where it is radiated away. As the companion inspirals, there may be interior regions where convection can effectively carry newly liberated orbital energy to the surface. The CE may then regulate itself with little-to-no orbital energy available for ejection until the companion reaches a region where the effects of convective transport no longer dominate.

To identify the convective regions of the primary star, we compute the convective velocities (v_{conv}) and scale heights (H) from our interior profiles when each star is at the maximum radial extent in its evolution. The convective timescale can then be estimated as,

$$t_{\text{conv}}[r] \sim 1.5H/v_{\text{conv}}[r]. \quad (2)$$

Similarly for each radius in the primary, we can determine the time required for the orbit to fully decay. This inspiral timescale is given as,

$$t_{\text{inspiral}}[r] = \int_{r_i}^{r_{\text{shred}}} \frac{\left(\frac{dM}{dr} - \frac{M[r]}{r}\right) \sqrt{v_r^2 + \bar{v}_\phi^2}}{4\xi\pi Gm_2 r \rho[r]} dr \quad (3)$$

where r_i is the initial radial position, r_{shred} is the tidal shredding radius which can be estimated via $r_{\text{shred}} \sim R_2 \sqrt[3]{2M_{\text{core}}/m_2}$, and $\bar{v}_\phi = v_\phi - v_{\text{env}} \simeq v_\phi$ for slow rotators such as RGB/AGB stars (Nordhaus et al. 2007). The parameter ξ accounts for the geometry of the companion's wake, the gaseous drag of the medium, and the Mach number (Park and Bogdanović 2017). We assume a value of $\xi = 4$, and note that the ejection efficiency is not sensitive to this value for the mass ratios considered in this work.

For regions in which the $t_{\text{conv}} \ll t_{\text{inspiral}}$, convection will transport orbital energy radially outward. If the turbulent region reaches an optically thin area such as the surface of the star, this energy can be lost via radiation. We refer to the convection region that makes contact with the surface of the star as the surface-contact convective region (SCCR). For lower mass stars in our sample ($\lesssim 3.0M_\odot$), there tends to be a single convective region at maximum extent. For stars more massive than $4.0M_\odot$, a deeper, yet physically distinct, secondary convective layer is also present (see Figure 1).

The inspiral and convective timescales are presented in Figure 1 for primary masses ranging from $1.0 - 6.0 M_\odot$ and companion masses ranging from $0.002 - 0.5 M_\odot$. SCCRs are shaded in yellow and secondary convective regions are shaded in pink. The tidal disruption locations are represented with X markers. The location and depth of the SCCR of the primary during inspiral is especially important and discussed in detail throughout the remainder of this paper.

2.2 Energy and Angular Momentum Considerations

The energy required to unbind the primary's envelope must be known to compute $\bar{\alpha}_{\text{eff}}$. By carrying out calculations directly from our stellar evolution models, we avoid employing λ -formalisms, which approximate the primary's gravitational binding energy for situations in which the interior structure is not known (De Marco et al. 2011). The minimum energy required to strip the envelope's mass exterior to a radius, r , is then given by:

$$E_{\text{bind}}[r] = - \int_M^{M_0} \frac{GM[r]}{r} dm[r], \quad (4)$$

where M_0 is the total mass of the primary star. One necessary, but not exclusive, condition for CE ejection is that the orbital energy

released during inspiral must exceed the binding energy of the envelope. Note that we focus exclusively on the gravitational component of the binding energy and do not include the internal energy of each shell in our calculations. While this could affect the ejection efficiency of the system, it has not been shown to make a significant contribution to the binding energy (Han et al. 1995; Ivanova et al. 2013).

The energy released via inspiral is given by

$$\Delta E_{\text{orb}}[r] = \frac{Gm_2}{2} \left(\frac{M_i}{r_i} - \frac{M[r]}{r} \right) \quad (5)$$

where m_2 is the companion's mass and r_i is the radius of the companion's orbit at the onset of energy transfer due to inspiral through the primary.

Equations 4 and 5 can then be combined with an efficiency to yield the following:

$$E_{\text{bind}} = \bar{\alpha}_{\text{eff}} \Delta E_{\text{orb}}, \quad (6)$$

where $\bar{\alpha}_{\text{eff}}$ is the effective efficiency of energy transfer to the envelope from the decaying orbit. If $\bar{\alpha}_{\text{eff}} = 1$, then all transferred orbital energy remains in the system and can fully contribute toward ejection. If $\bar{\alpha}_{\text{eff}} = 0$, no orbital energy remains in the system and the CE would never be ejected. We discuss $\bar{\alpha}_{\text{eff}}$ in the context of models and their convective zones in detail in Section 3.

As the companion mass inspirals through the envelope of the primary star, its decreasing orbital separation transfers angular momentum to the CE, thereby spinning it up. The change of angular momentum of the envelope's spherical layers is given as:

$$\Delta L_{\text{env}}[r] = \frac{2}{3} M[r] v_{\text{env}} r, \quad (7)$$

where v_{env} is the envelope's velocity after inspiral. We have taken the envelope's initial angular momentum to be zero, a reasonable assumption for slow rotators such as RBG and AGB stars. The change of angular momentum of a companion is given by:

$$\Delta L_{m_2}[r] = m_2(v_\phi r - v_{\phi,i} r_i), \quad (8)$$

where $v_{\phi,i}$ and v_ϕ are the initial and final Keplerian orbital velocities of the companion, respectively.

By equating Equations 7 and 8, angular momentum is conserved and the velocity of the envelope can be written as:

$$v_{\text{env}}[r] = \frac{3\sqrt{G}}{2} \frac{\left(\sqrt{M[r]r} - \sqrt{M[r_i]r_i}\right)}{M[r]r} m_2. \quad (9)$$

The envelope velocity calculated for specific radii is compared to the Keplerian velocity at the same respective radii. From this, it can be determined whether or not the envelope has enough angular momentum to spin faster than a Keplerian orbit and consequently move radially outward. Note that angular momentum constraints do not guarantee ejection as material will move to larger radii where it may still be bound. Results from our models are discussed in Section 3.3.

2.3 Common Envelope Outcomes

There are two possible outcomes for common envelope phases: (i.) the companion survives the interaction and emerges in a short-period, post-CE binary, or (ii.) it does not and is destroyed in the process.

The companion body's radius, R_2 , is estimated according to its mass. For planet-mass objects ($m_2 \leq 0.0026M_\odot$, Zapolsky and Salpeter 1969) the radius is approximated as $R_2 = R_{\text{Jupiter}}$. For

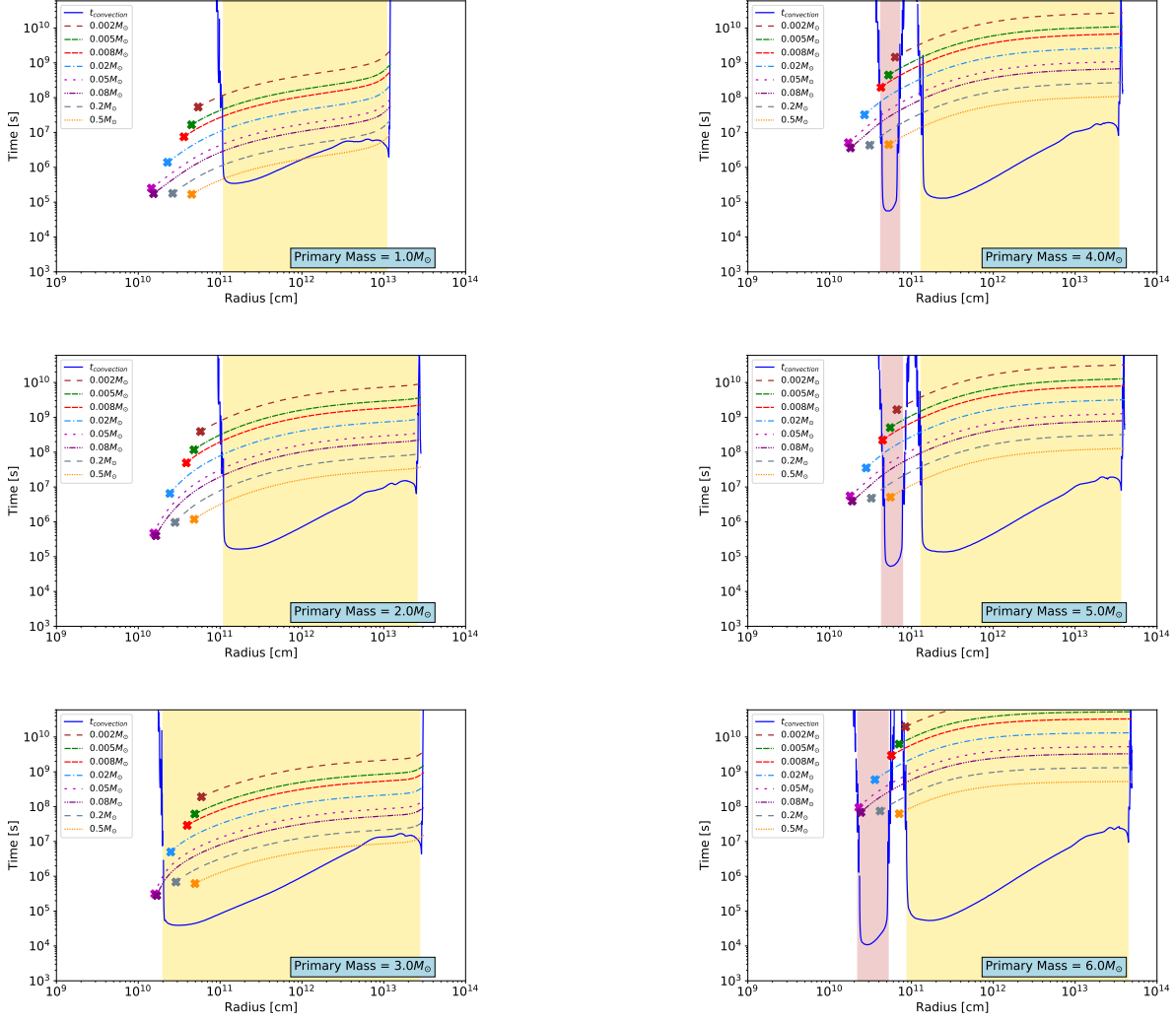


Figure 1. Comparative timescale plots for a sample of representative primary masses at their maximum radial extent and several test companion masses. The convective timescale profile of the primary star is shown in solid blue. The coloured, dashed lines show the inspiral timescale - the time it takes for the companion mass to spiral from its current radius to the centre of the primary star. The radius at which each companion mass shreds due to the gravity of the primary mass is marked with an X. The surface-contact convective regions (SCCRs) of the primary star that do not contribute to the unbinding of the envelope are shaded in yellow. Interior convective zones that do not extend to the primary’s surface are shaded in pink.

brown dwarfs ($0.0026M_{\odot} < m_2 < 0.077M_{\odot}$, Burrows et al. 1993), the radius is calculated via:

$$R_2/R_{\odot} = 0.117 - 0.054 \log^2 \left(\frac{m_2}{0.0026M_{\odot}} \right) + 0.024 \log^3 \left(\frac{m_2}{0.0026M_{\odot}} \right)$$

(Reyes-Ruiz and Lopez 1999). For stellar companions ($m_2 \geq 0.077M_{\odot}$), a power law is used:

$$R_2 = \left(\frac{m_2}{M_{\odot}} \right)^{0.92} R_{\odot} \quad (10)$$

(Reyes-Ruiz and Lopez 1999).

To determine whether a companion survives the CE and emerges in a short-period orbit, there must exist an orbital separation, a , such that: (i.) $\bar{\alpha}_{\text{eff}} \Delta E_{\text{orb}}[a] > E_{\text{bind}}[a]$ and (ii.) $a > r_{\text{shred}}$. The shredding radius of each companion mass is determined as described in Section 2.1. The shredding radii are presented as X symbols in Figures 1 and 2. If the companion disrupts early in its

descent through the envelope, the energy available to unbind the envelope will be minimized, whereas if the companion body remains intact through the majority of the envelope, the opposite will be true. This is discussed in more detail in Section 3.

3 EJECTION EFFICIENCY IN CONVECTIVE REGIONS

The efficiency with which orbital energy can be used to unbind the envelope is a function of position inside the CE. To determine a lower limit for $\bar{\alpha}_{\text{eff}}$ in a star with convective regions, we proceed in the following manner. If $t_{\text{conv}} < t_{\text{inspiral}}$, and the companion is orbiting inside a surface-contact convective region (SCCR), then there is no contribution to $\bar{\alpha}_{\text{eff}}$ as the orbital energy can be transported via convection to the surface and leave the system as photons. If the companion is orbiting in a region where $t_{\text{inspiral}} < t_{\text{conv}}$,

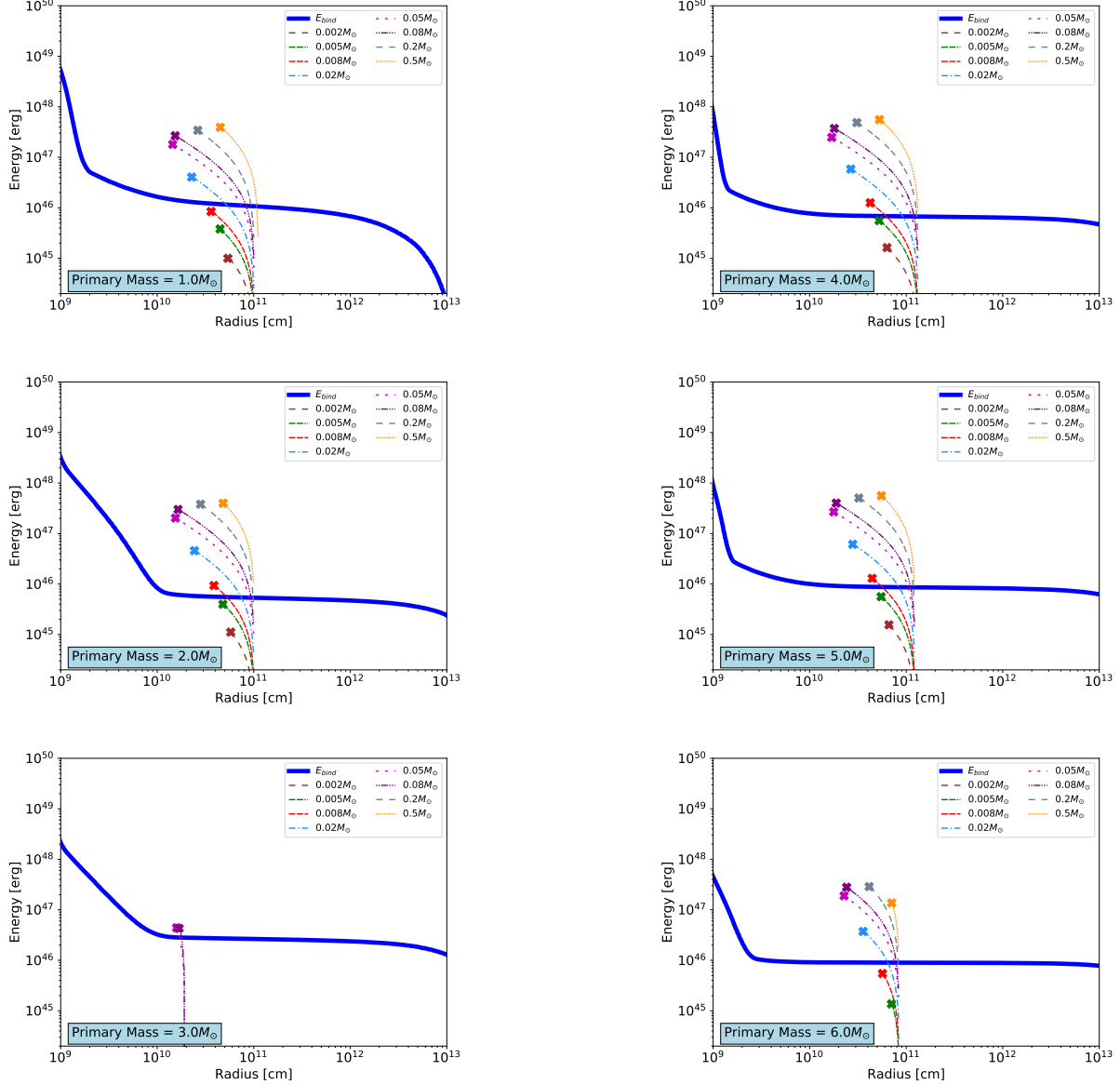


Figure 2. Comparative energy plots for a sample of representative primary masses at their maximum radial extent and several test companion masses. The binding energy for the primary star is shown in solid blue. The coloured, dashed lines show the change in orbital energy of the companion star as it inspirals, and the radius at which the companion shreds is marked with an X. (Several X's in the $3.0M_{\odot}$ plot fall below 10^{44} erg.) For companion masses which the X falls below the binding energy curve, the companion will disrupt during inspiral before enough energy is transferred to unbind the envelope of the primary. These orbital energy curves take into account the convective zones of the primary, in that movement through the surface-contact convective regions (SCCRs) does not contribute energy to the ejecting of the envelope.

then the orbital energy cannot escape the system and fully contributes, in some form, toward raising the negative binding energy of the primary. In this way, we construct an average ejection efficiency by determining individual binary α_{eff} coefficients (0 or 1) at each position. We designate regions within the SCCR to have $\alpha_{\text{eff}} = 0$, as the energy can be carried to an optically thin layer and radiated away; we designate all other regions to have $\alpha_{\text{eff}} = 1$, as we assume that the energy transferred by the change in orbital energy of the companion gets evenly distributed throughout the mass in each radial shell. Then for each primary-companion pair, we de-

termine $\bar{\alpha}_{\text{eff}}$ by integrating from the surface to the point of tidal disruption via:

$$\bar{\alpha}_{\text{eff}} = \frac{\int_{r_o}^{r_{\text{shred}}} \alpha_{\text{eff}}[r] dE_{\text{orb}}[r]}{E_{\text{orb}}[r_{\text{shred}}] - E_{\text{orb}}[r_o]}, \quad (11)$$

where $dE_{\text{orb}}[r]$ can be calculated discretely as in Equation 5.

Note that we assume the internal structure of the primary is constant during inspiral. Since orbital energy is a function of enclosed mass of the primary and position, liberated orbital energy is distributed to the mass present in each location.

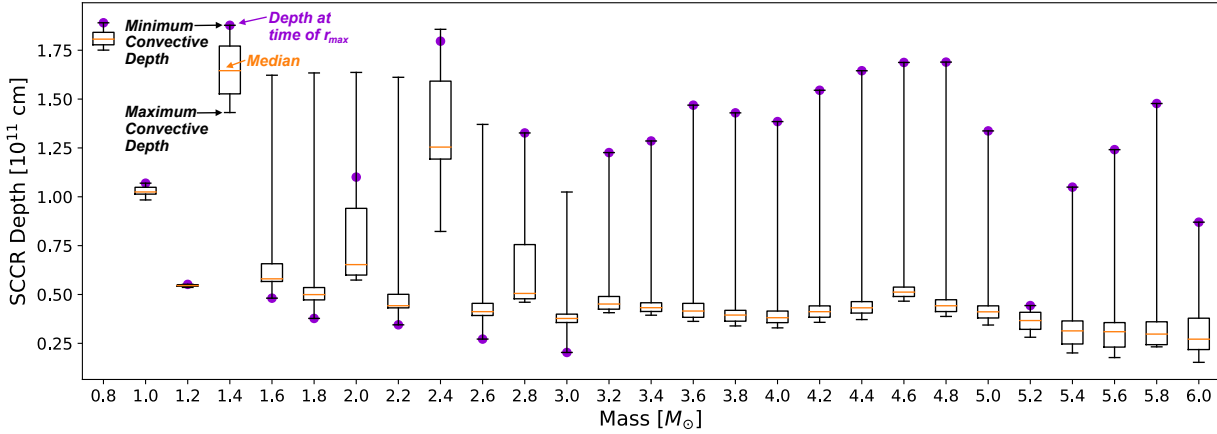


Figure 3. Box-and-whisker plot shows the range of convective depths during the final thermal pulse of the primary mass just prior to and including the time of maximum radius (does not include any time after the maximum radius). The orange line inside the box shows the median value of the boxplot, the vertical extent of the box marks the interquartile range (IQR: the middle 50% of the range), and the upper and lower bounds of the whiskers mark the minimum and maximum convective depths, respectively. Note that for primary masses below $1.4M_{\odot}$ the spanned range is very small, showing a stable convective region.

The curves showing E_{bind} and ΔE_{orb} for primaries between $1.0 - 6.0M_{\odot}$ and companions between $0.002 - 0.5M_{\odot}$ can be seen in Figure 2. Each subplot shows the binding energy of the primary (thick blue line), compared with the change in orbital energy of several companions, in dashed, coloured lines. The transfer of the released orbital energy is halted by the SCCR ($\alpha_{\text{eff}} = 0$), resulting in low, unchanging values of E_{orb} , and resumes once the companion has inspiraled deeper than the lower boundary of the SCCR ($\alpha_{\text{eff}} = 1$). The radius at which the companion tidally shreds is marked with an X symbol, halting energy transfer.

On the six subplots in Figure 2, the location of the X-symbols show which companion masses unbind the envelope; if the X falls above the solid blue E_{bind} curve, the companion survives the inspiral and emerges as a post-CE binary in a short-period orbit. We see that for a representative SCCR depth of 10^{11} cm, companions between $0.008 - 0.02M_{\odot}$ ($\sim 8 - 20M_{\text{Jupiter}}$) and greater will successfully unbind the envelope and survive the binary interaction.

3.1 Variability of the SCCR

As described in Section 2.1, we argue that mixing of the energy released by the inspiraling companion occurs within the convective regions of the primary star, with emphasis on the potential for the SCCR to carry energy that is then radiated away. Therefore, an understanding of the variability of the SCCR is imperative to a complete understanding of patterns in the ejection efficiency. An examination of the stability of the SCCR with mass is shown in Figure 3. This box-and-whisker plot displays the range of convective depths of the SCCR during the final thermal pulse of all monitored primary masses (boxes and whiskers), the median SCCR depth (orange line), and the SCCR depth at the time of maximum radius (purple circle).

The variability of the SCCR becomes evident first in the $1.4M_{\odot}$ model and the range of SCCR depths remains large for all greater primary masses. The primary’s time of maximum radius consistently corresponds with the minimum convective depth following and including the $3.2M_{\odot}$ model, thus maximizing $\bar{\alpha}_{\text{eff}}$. For the instances where the SCCR is at maximum depth and maximum

radius concurrently, the companion tidally shreds within the deep SCCR or shortly thereafter, minimizing $\bar{\alpha}_{\text{eff}}$.

The SCCR depth over time is of interest because of its inconsistency at the time of maximum radius, which is evident in Figure 3. The SCCR depth of three representative models are plotted over time and can be seen in Figure 4. The $1.0M_{\odot}$ model, $1.8M_{\odot}$ model, and $4.6M_{\odot}$ model are representative of a stable SCCR, a maximum-SCCR-depth-at- r_{max} SCCR, and a *minimum*-SCCR-depth-at- r_{max} SCCR, respectively. The depth of the SCCR over time is plotted in the coloured, dashed lines. The respective radii of the primary over time are shown in blue, with dash patterns identical to those for the companion-mass SCCR depths. The look-back time is normalized to the maximum age of the star, and centred around the time of r_{max} , $t = 0$. Each tick of normalized look-back time corresponds to a duration on the order of $\sim 10^2$ years. For the $1.8M_{\odot}$ model, the time of peak radius corresponds with the time of deepest SCCR, thus minimizing the $\bar{\alpha}_{\text{eff}}$ value. The $1.0M_{\odot}$ SCCR depth remains remarkably constant, and the depth of the $4.6M_{\odot}$ SCCR decreases with time, in stark contrast to that of the $1.8M_{\odot}$ model. Companions will have been engulfed by r_{max} or will never be engulfed. Therefore, though the SCCR depth of the $4.6M_{\odot}$ model continues to decrease during the time after r_{max} (see Fig. 4), the SCCR is considered at “minimum depth” in Figure 3 as the interior structure of the primary is only of interest prior to and including the time at maximum radial extent.

3.2 Ejection Efficiency, $\bar{\alpha}_{\text{eff}}$

The ejection efficiency is unique for each primary-companion mass pair, since $\bar{\alpha}_{\text{eff}}$ depends on the specific internal stellar structure (especially properties of the SCCR) and the properties of the companion. We calculate $\bar{\alpha}_{\text{eff}}$ values for a matrix of primary-companion pairs and present the results in Figure 5.

The slight vertical colour trend seen at $m_2 = 0.06M_{\odot} - 0.08M_{\odot}$ is due to the transition from sub-stellar to stellar companion and the corresponding change in density. As the density of the companion increases, the shredding radius decreases. It follows that a denser companion will inspiral further into the primary’s envelope before disrupting than a less dense companion. It is only the

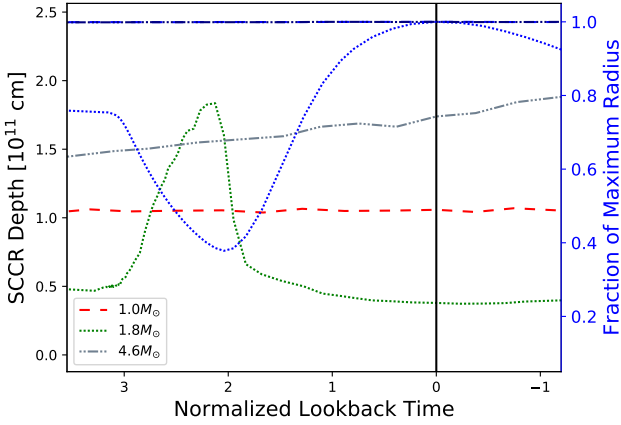


Figure 4. The SCCR depths over time are shown along with the primary’s radius for three representative primary masses. The x-axis is a lookback time until maximum radius, described by: $\frac{t[r_{\max}] - t[r]}{t[r_{\max}]}$. The vertical black line marks the time of r_{\max} , $t = 0$. (Times after maximum radius are shown here for completeness but are not examined in this work.) The blue lines show the fraction of maximum radius in time. Two of the three blue lines overlap at unity. The coloured, dashed lines show the SCCR depth over time. Note the instability in the convective zone as it approaches the maximum radius for the $1.8M_{\odot}$ model. (Convective depth is maximized with decreased interior convective radius.)

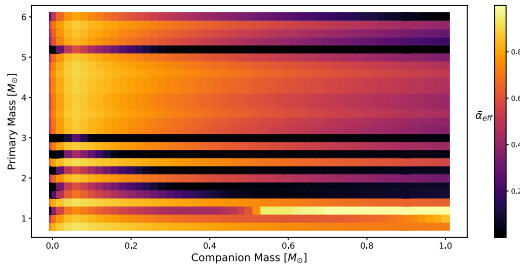


Figure 5. Colourmap of effective ejection efficiencies ($\bar{\alpha}_{\text{eff}}$) based on surface-contact convective regions (SCCRs) of the primary star.

distance that companions survive past the SCCR that contributes non-zero values to $\bar{\alpha}_{\text{eff}}$.

The distinct horizontal stripes between primary masses of $1.2M_{\odot}$ and $3.0M_{\odot}$ are particularly evident. This phenomenon can be attributed to variability of the SCCR during the final thermal pulse ($\sim 10^2$ years) of the primary star thus making the ejection efficiency sensitive to the time of the CE phase.

3.3 Envelope Spin

The rotational velocity of the outermost layers of the star, the envelope, are assumed to be initially stationary. Using the method described in Section 2.3, the angular momentum transfer of each companion mass is compared to the angular momentum of the envelope and, using Eq. 9, the envelope velocity is found. That velocity is then compared to the Keplerian velocity, v_{ϕ} , of the corresponding radius away from the centre of the primary.

These comparisons can be seen in Figure 6, which shows the Keplerian velocities of the $1.0M_{\odot}$ and $6.0M_{\odot}$ models in the thick

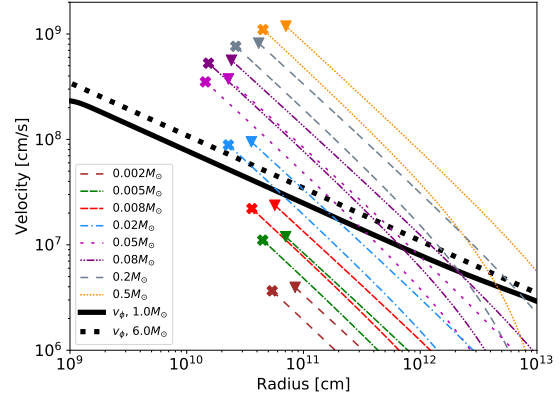


Figure 6. Induced envelope velocity as companions move through radii of the primary compared to Keplerian velocity. The coloured, dashed lines represent the envelope velocity curves based on angular momentum transfer from companions inspiraling through the $1.0M_{\odot}$ (X’s) and $6.0M_{\odot}$ (triangles, \blacktriangledown) models. The X or triangle marks the shredding radius of the companion. All envelope velocities for primaries within this mass range fall between the respective companions’ curves. The black lines show the Keplerian velocity at a given radius based on enclosed mass. If the X or triangle falls above the black line, the envelope spins *faster* than Keplerian, and will thus begin to move away from the core of the star.

black solid and dotted lines, respectively. Atop the Keplerian velocities in dashed, coloured lines are the envelope velocities as induced by the transferred angular momentum of companion masses between $0.002 - 0.5M_{\odot}$.

We provide the induced envelope rotation rates for $1.0M_{\odot}$ and $6.0M_{\odot}$ primaries. The range of Keplerian velocities for all primary masses in the sample remain within the plotted limits; for primaries in this sample, all envelope spin velocities induced by companion masses also fall within the range of the two models shown. The velocity induced by inspiraling companions greater than $0.02M_{\odot}$ exceeds the minimum velocity necessary to spin-up the envelope past Keplerian and push material outward.

4 DISCUSSION OF RESULTS

In comparison to observational results presented by De Marco et al. (2011) and Zorotovic et al. (2011), we plot the $\bar{\alpha}_{\text{eff}}$ vs. $q = m_2/M_1$ relation found from our simulated data in Figure 7. The top panel is limited to the parameter space considered by De Marco et al. while the parameter space for our full suite of primary-companion mass pairs are shown in the bottom panel. Within the range of De Marco et al., most of our ejection efficiencies do show an anti-correlation with mass ratio but with varying slopes. Zorotovic et al. (2011) are, however, in disagreement with De Marco et al., finding larger final separations with lower companion masses. In the lower panel of Figure 7, in which we present our full results, there are regions of parameter space that positively correlate with mass ratio.

It is worthwhile to note that De Marco et al. and Zorotovic et al. estimate $\bar{\alpha}_{\text{eff}}$ through observations of assumed CE progenitors, whereas we use stellar evolution models to probe the interior structure of primaries during the CE phase. For this reason, we note that a direct comparison is difficult as both studies estimate the CE binding energy via a λ parameter. This can result in ejection effi-

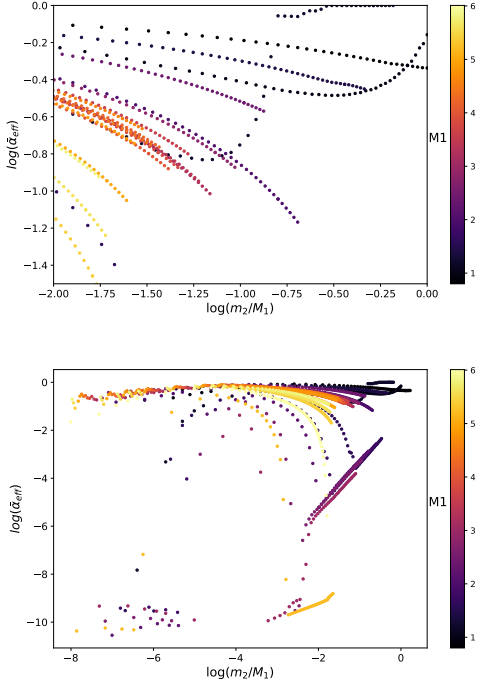


Figure 7. Top: Axis-constrained mass ratio and corresponding $\bar{\alpha}_{\text{eff}}$. These axis limits are comparable to the parameter space examined by De Marco et al. (2011), who also found a negative slope in this range. Bottom: Mass ratio and $\bar{\alpha}_{\text{eff}}$ for all primary-companion mass pairs in this study.

iciencies that are greater than unity making direct comparison challenging.

Politano and Weiler (2007) argue that $\bar{\alpha}_{\text{eff}}$ is a function of the companion mass and the interior structure of the evolved primary, a statement with which we agree. Through this work, we find that the ejection efficiency is, in fact, highly sensitive to properties of the convective regions of the primary during the CE phase. To simulate CE systems and find the $\bar{\alpha}_{\text{eff}}$ value, one must consider the effect of mixing within convective regions.

Convective mixing can affect the system in different ways depending on where it occurs. As the companion inspirals, convection can transport the released orbital energy away from the companion and distribute it throughout other regions. If convection occurs in the SCCR, then the convective eddies can carry the energy to the surface where it can be radiated away. This work assumes that all orbital energy released within the SCCR is radiated away and thus provides a lower limit on $\bar{\alpha}_{\text{eff}}$ under the assumption that the liberated orbital energy is distributed evenly among the mass in a given layer.

In some cases, the $\bar{\alpha}_{\text{eff}}$ value of a specific system may deviate a bit from the values presented here, due to internal structure changes during inspiral (the depth of the SCCR can vary on $\sim 10^2$ year timescales, as in Figure 4, and the estimated duration of the entire CE phase is of comparable length). For this work, we assumed the internal structure to remain constant once the companion was engulfed. In any case, $\bar{\alpha}_{\text{eff}}$ is sensitive to the time of the companion’s inspiral through the envelope of primary, since the SCCR varies so rapidly during the evolution of a star. For this work, we used the profile of a primary at its maximum radius, and assumed that the secondary began to skim the primary’s surface at that time. We chose this because at the maximum extent of the primary, the

largest spatial volume in which tidal dissipation may lead to CE phases is the greatest. Given our findings of the dependence of the quickly-changing SCCR, the ejection efficiency values shown in Figure 5 cannot be generalized to those companion-mass pairs. Instead, the SCCR of the primary at the specific time of companion’s engulfment must be known to calculate ejection efficiencies for unique configurations.

4.1 Implications of Convection

Convection allows the binary to naturally shrink to sub-day orbital periods before the liberated orbital energy can be tapped to drive ejection. This is, at least at initial glance, consistent with the steep drop off in observed post-CE systems that have orbital periods greater than a day (Davis et al. 2010). Investigating the predicted post-CE population distributions when $\bar{\alpha}_{\text{eff}}$ from Equation 11 is adopted is an interesting future direction but requires determining when common envelope evolution starts.

The rate of orbital decay in some numerical simulations is slowed due to the gas reaching co-rotation (Ricker and Taam 2012; Ohlmann et al. 2016; Chamandy et al. 2018a). However, co-rotation cannot be perfectly maintained in a turbulent medium and thus may lead to faster decay than is currently seen in numerical work. If the orbital decay time remains above the convective turnover time in the SCCR, then the effect will be minimal as energy transport to the surface is the dominant process.

In regions where the orbital decay timescale is shorter than the convective turnover times, $\alpha_{\text{eff}}[r] = 1$. In principle, this means that we are implicitly assuming that the orbital energy is equally distributed to the mass in that region. At the inner boundary of the SCCR where this condition is satisfied, turbulent mixing may distribute sufficient orbital energy to enough of the mass to eject the full envelope. Primaries with masses $> 3.0M_{\odot}$ have secondary convective zones that may also aid in mixing sufficient orbital energy for those companions that reach it before being disrupted. These assumptions warrant investigation via numerical simulations that include convection (see Chamandy et al. 2018b for further discussion).

5 CONCLUSIONS AND FUTURE DIRECTIONS

We have studied the effects of convection on the ejection efficiencies of common envelope interactions. Using detailed stellar evolution models at the time of maximal radial extent, we calculate $\bar{\alpha}_{\text{eff}}$ values for a matrix of primary-companion mass pairs. The ejection efficiencies are most sensitive to the properties of the surface-contact convective region (SCCR). In this region, the orbital decay timescales are longer than the convective turnover timescales, thereby allowing the star to effectively radiate released orbital energy and thus lower $\bar{\alpha}_{\text{eff}}$. The inclusion of convection in CEs may solve the ejection problem seen in numerical simulations without the need for additional energy sources as the orbit must decay substantially before orbital energy can be tapped to drive ejection. Our considerations of convection also allow for post-CE orbital periods of less than a day, an observational result that has been infrequently reproduced in population synthesis models that use universal, or constant, ejection efficiencies.

We provide a simple method to calculate $\bar{\alpha}_{\text{eff}}$ if the properties of the SCCR are known. Since the ejection efficiencies are sensitive to the depth of the SCCR, they are inherently sensitive to the time of engulfment. If the SCCR depth changes substantially over time

for a given stellar evolution model, then the time of the CE onset will determine the ejection efficiency. However, since RGB/AGB stars possess deep convective envelopes, the effects of convection remain important, independent of when a CE commences.

Future work can be advanced on multiple fronts. Numerical work should include high-resolution simulations of convection in common envelopes. Since this may be challenging in global simulations without convective sub-grid models, high-resolution local simulations of convective energy transport in stratified wind tunnels may be a natural starting point (MacLeod et al. 2017). Massive stars also host deep convective zones and the impact on the ejection efficiencies should be investigated in the context of formation channels for the progenitors of gravitational-wave driven, compact-object mergers (Belczynski et al. 2016). Finally, coupling these calculations to dynamical calculations that determine the time of engulfment can result in improved ejection efficiencies, which could then be incorporated into studies of populations (Belczynski et al. 2002; Moe and De Marco 2006).

ACKNOWLEDGEMENTS

ECW and JN acknowledge support from the following grants: NASA HST-AR-15044, NASA HST-AR-14563 and NTID SPDI-15992. The authors thank Gabriel Guidarelli, Jeff Cummings, Joel Kastner, Luke Chamandy, Eric Blackman, John Whelan and Adam Frank for stimulating discussions.

REFERENCES

- Belczynski, K., Holz, D. E., Bulik, T., and O’Shaughnessy, R.: 2016, *Nature* **534**, 512
- Belczynski, K., Kalogera, V., and Bulik, T.: 2002, *ApJ* **572**, 407
- Bloecker, T.: 1995, *A&A* **297**, 727
- Burrows, A., Hubbard, W. B., Saumon, D., and Lunine, J. I.: 1993, *The Astrophysical Journal* **406**, 158
- Canals, P., Torres, S., and Soker, N.: 2018, *MNRAS* **480**, 4519
- Chamandy, L., Frank, A., Blackman, E. G., Carroll-Nellenback, J., Liu, B., Tu, Y., Nordhaus, J., Chen, Z., and Peng, B.: 2018a, *MNRAS* **480**, 1898
- Chamandy, L., Yisheng, T., Blackman, E. G., Carroll-Nellenback, J., Frank, A., Liu, B., and Nordhaus, J.: 2018b, *in prep*
- Chen, Z., Frank, A., Blackman, E. G., Nordhaus, J., and Carroll-Nellenback, J.: 2017, *MNRAS* **468**, 4465
- Claeys, J. S. W., Pols, O. R., Izzard, R. G., Vink, J., and Verbunt, F. W. M.: 2014, *A&A* **563**, 83
- Cojocaru, R., Rebassa-Mansergas, A., Torres, S., and García-Berro, E.: 2017, *MNRAS* **470**, 1442
- Davis, P. J., Kolb, U., and Willems, B.: 2010, *Monthly Notices of the Royal Astronomical Society* **403(1)**, 179
- De Marco, O., Passy, J.-C., Moe, M., Herwig, F., Low, M.-M. M., and Paxton, B.: 2011, *Mon. Not. R. Astron. Soc* **411**, 2277
- Fabrycky, D. and Tremaine, S.: 2007, *ApJ* **669**, 1298
- Glanz, H. and Perets, H. B.: 2018, *MNRAS* **478**, L12
- Grichener, A., Sabach, E., and Soker, N.: 2018, *Monthly Notices of the Royal Astronomical Society* **478(2)**, 1818
- Han, Z., Podsiadlowski, P., and Eggleton, P. P.: 1995, *MNRAS* **272**, 800
- Iben, I. and Livio, M.: 1993, *December Common Envelopes in Binary Star Evolution I*, Technical report
- Iben, I., J. and Tutukov, A. V.: 1984, *The Astrophysical Journal* **284**, 719
- Ivanova, N.: 2018, *ApJL* **858**, L24
- Ivanova, N., Justham, S., Avendano Nandez, J. L., and Lombardi, J. C.: 2013, *Science* **339**, 433
- Ivanova, N., Justham, S., Chen, X., De Marco, O., Fryer, C. L., Gaburov, E., Ge, H., Glebbeek, E., Han, Z., Li, X. D., Lu, G., Marsh, T., Podsiadlowski, P., Potter, A., Soker, N., Taam, R., Tauris, T. M., Van Den Heuvel, E. P., and Webbink, R. F.: 2013, *Astronomy and Astrophysics Review* **21(1)**
- Ivanova, N., Justham, S., and Podsiadlowski, P.: 2015, *MNRAS* **447**, 2181
- Kashi, A. and Soker, N.: 2018, *MNRAS* **480**, 3195
- Kochanek, C. S., Adams, S. M., and Belczynski, K.: 2014, *MNRAS* **443**, 1319
- Kruckow, M. U., Tauris, T. M., Langer, N., Kramer, M., and Izzard, R. G.: 2018, *MNRAS* **481**, 1908
- Kuruwita, R. L., Staff, J., and De Marco, O.: 2016, *MNRAS* **461**, 486
- Livio, M. and Soker, N.: 1988, *The Astrophysical Journal* **329**, 764
- MacLeod, M., Antoni, A., Murguia-Berthier, A., Macias, P., and Ramirez-Ruiz, E.: 2017, *ApJ* **838**, 56
- MacLeod, M., Ostriker, E. C., and Stone, J. M.: 2018, *ApJ* **863**, 5
- Moe, M. and De Marco, O.: 2006, *ApJ* **650**, 916
- Nordhaus, J. and Blackman, E. G.: 2006, *Monthly Notices of the Royal Astronomical Society* **370(4)**, 2004
- Nordhaus, J., Blackman, E. G., and Frank, A.: 2007, *MNRAS* **376**, 599
- Nordhaus, J. and Spiegel, D. S.: 2013, *MNRAS* **432**, 500
- Nordhaus, J., Spiegel, D. S., Ibgui, L., Goodman, J., and Burrows, A.: 2010, *MNRAS* **408**, 631
- Nordhaus, J., Wellons, S., Spiegel, D. S., Metzger, B. D., and Blackman, E. G.: 2011, *Proceedings of the National Academy of Science* **108**, 3135
- Ohlmann, S. T., Röpkke, F. K., Pakmor, R., and Springel, V.: 2016, *The Astrophysical Journal* **816(1)**, L9
- Paczynski, B.: 1976, in P. Eggleton, S. Mitton, and J. Whelan (eds.), *Structure and Evolution of Close Binary Systems*, Vol. 73, pp 75–80, Dordrecht: Reidel, iau sympos edition
- Park, K. and Bogdanović, T.: 2017, *The Astrophysical Journal* **838(2)**, 103
- Passy, J. C., De Marco, O., Fryer, C. L., Herwig, F., Diehl, S., Oishi, J. S., Mac Low, M. M., Bryan, G. L., and Rockefeller, G.: 2012, *Astrophysical Journal* **744(1)**, 52
- Paxton, B., Bildsten, L., Dotter, A., Herwig, F., Lesaffre, P., and Timmes, F.: 2011, *ApJS* **192**, 3
- Paxton, B., Schwab, J., Bauer, E. B., Bildsten, L., Blinnikov, S., Duffell, P., Farmer, R., Goldberg, J. A., Marchant, P., Sorokina, E., Thoul, A., Townsend, R. H. D., and Timmes, F. X.: 2018, *ApJS* **234**, 34
- Politano, M. and Weiler, K. P.: 2007, *The Astrophysical Journal* **665(1)**, 663
- Reimers, D.: 1975, *Memoires of the Societe Royale des Sciences de Liege* **8**, 369
- Reyes-Ruiz, M. and Lopez, J. A.: 1999, *The Astrophysical Journal* **524(2)**, 952
- Ricker, P. M. and Taam, R. E.: 2012, *The Astrophysical Journal* **746(8pp)**, 74
- Sabach, E., Hillel, S., Schreier, R., and Soker, N.: 2017, *Monthly Notices of the Royal Astronomical Society* **472(4)**, 4361
- Shappee, B. J. and Thompson, T. A.: 2013, *ApJ* **766**, 64

- Soker, N.: 2015, *ApJ* **800**, 114
Soker, N., Grichener, A., and Sabach, E.: 2018, *ApJL* **863**, L14
Thompson, T. A.: 2011, *ApJ* **741**, 82
Toonen, S. and Nelemans, G.: 2013, *Astronomy & Astrophysics* **557**, A87
Tutukov, A. and Yungelson, L.: 1979, in P. Conti and C. de Loore (eds.), *Mass Loss and Evolution of O-Type Stars*, pp 401–407, Reidel Publishing Company, Dordrecht, iau sympos edition
Villaver, E. and Livio, M.: 2009, *ApJL* **705**, L81
Webbink, R. F.: 1984, *The Astrophysical Journal* **277**, 355
Zapolsky, H. S. and Salpeter, E. E.: 1969, *The Astrophysical Journal* **158**, 809
Zorotovic, M., Schreiber, M., Gänsicke, B., Rebassa-Mansergas, A., Nebot Gómez-Morán, A., Southworth, J., Schwöpe, A., Pyrzas, S., Rodríguez-Gil, P., Schmidtobreick, L., Schwarz, R., Tappert, C., Toloza, O., and Vogt, N.: 2011, *A&A* **536**, L3
Zorotovic, M., Schreiber, M. R., Gänsicke, B. T., and Nebot Gómez-Morán, A.: 2010, *A&A* **520**, 86